Collective Coupling of a Macroscopic Number of Single-Molecule Magnets with a Microwave Cavity Mode

A. W. Eddins,[1,*] C. C. Beedle,[2,†] D. N. Hendrickson,[2] and Jonathan R. Friedman[1,‡]
[1]Department of Physics, Amherst College, Amherst, Massachusetts 01002-5000, USA
[2]Department of Chemistry & Biochemistry, University of California at San Diego, La Jolla, California 92093, USA
(Received 22 July 2013; revised manuscript received 8 September 2013; published 26 March 2014)

We report the observation of strong coupling of a macroscopic ensemble of $\sim 10^{16}$ Fe_8 molecular nanomagnets to the resonant mode of a microwave cavity. We use millimeter-wave spectroscopy to measure the splitting of the system's resonant frequency induced by the coupling between the spins and the cavity mode. The magnitude of this splitting is found to scale with $\sqrt{N}$, where N is the number of collectively coupled spins. We control N by changing the system's temperature and, thereby, the populations of the relevant spin energy levels. Strong coupling is observed for two distinct transitions between spin energy states. Our results indicate that at low temperatures nearly all of the spins in the sample couple with the cavity's resonant mode even though there is substantial inhomogeneous broadening of the Fe_8 spin resonances.

DOI: 10.1103/PhysRevLett.112.120501 PACS numbers: 03.67.Lx, 42.50.Pq, 75.50.Xx, 76.30.-v

For two decades, single-molecule magnets (SMMs) have held promise to become an ultrahigh-density magnetic storage medium [1], and there has been significant recent progress towards realizing this goal [2]. In tandem, because SMMs are quantum systems [3], they have been suggested as possible qubits [4]. Quantum coherent phenomena have been observed in several SMM systems [5–8] with some exhibiting coherence times on the order of 1–10 μs. There has also been major progress in addressing individual SMMs [9–16]. Alternatively, SMMs may be employed as a form of quantum memory within a hybrid quantum processor [17–21] in which quantum information is stored holographically in the entire crystal rather than bitwise in individual molecules. A first step towards implementing such a scheme with SMMs is to demonstrate that SMMs can quantum coherently couple to the photon states of a resonant cavity. Here we present spectroscopic evidence that nearly all of the $\sim 10^{16}$ molecules in a crystal of the Fe_8 SMM collectively couple with a resonant cavity mode. We find that the strength of the coupling scales with $\sqrt{N}$, where N is the number of collectively coupled spins, a parameter that depends on the system's temperature. Our results indicate that such collective coupling occurs even though there is substantial inhomogeneous broadening of the Fe_8 spin resonances.

Coherent coupling between two-level systems (e.g., spins) and cavity photons lies at the heart of cavity quantum electrodynamics. Such interactions have been seen in many systems, including individual atoms [22], Bose-Einstein condensates [23], semiconductor quantum dots [24,25], and superconducting qubits [26]. In each of those systems the coupling is via electric-dipole transitions. Recently, coupling cavity photons to spins via magnetic dipole transitions has been investigated [27]. This weaker coupling, while more challenging to observe, may lead to longer coherence times. Coupling of spins and cavity photons has been observed in several low-spin systems, including standard electron-spin resonance materials [28,29], nitrogen-vacancy centers in diamond [21,30,31], N-doped buckyballs [32], Cr^{3+} impurities in ruby [33], as well as other magnetically doped materials [32,34,35]. In all of these systems the spin belongs to a single atom, ion, or nucleus. In contrast, SMMs are more "macroscopic" artificial magnets where the spin degree of freedom is a joint property of an entire metal-oxide molecular cluster. These magnets have a large magnetic anisotropy, which produces a sizeable zero-field splitting between spin states. This enables coupling the spins to microwave photons at low magnetic fields, making some SMMs (with appropriate anisotropy values) potentially integrable with superconducting resonators and qubit circuits, which cannot operate at high fields. The macroscopic nature of SMMs presents a complication: For many SMMs, variations in the local environment of the molecules within a crystal lead to slightly different properties for each molecule [36] and inhomogeneous broadening of spectral resonance lines [37]. At the same time, with $\sim$1 molecule per unit cell and a large ($s \sim 10$) magnetic moment, SMMs also have an extremely high spin density, leading to a much stronger spin-photon interaction than what is seen in many other spin systems. Our results show that the high spin density in SMMs can be harnessed to create a coupling strong enough to overcome the intrinsic inhomogeneity of the system.

The Fe_8 molecule [Fig. 1(c)] is a spin-10 object with a large magnetocrystalline anisotropy, resulting in a preferred orientation for the spin, the so-called "easy" axis. As the spin tilts away from this axis, its energy increases, creating an effective double-well potential [Fig. 1(a)] as a function of the angle between the spin and the easy axis. The Fe_8 spin Hamiltonian is given by

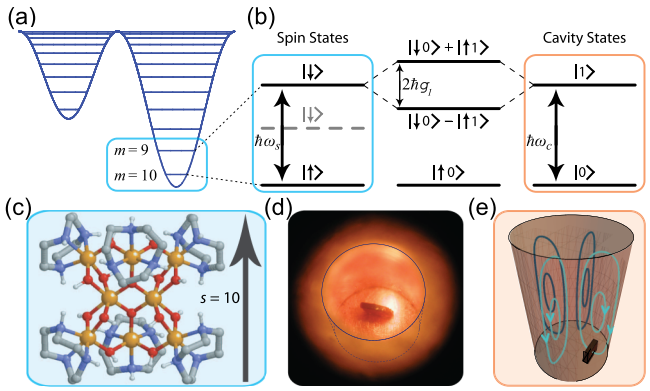

FIG. 1 (color online). (a) Double-well potential for a single-molecule magnet in a magnetic field. The levels correspond to different spin-orientation states. (b) Schematic of spin-photon interaction. One pair of SMM levels (the lowest two for the case shown) are labeled $|\uparrow\rangle$ and $|\downarrow\rangle$, as shown. Photon-number states are labeled $|0\rangle$ and $|1\rangle$. A magnetic field causes the excited state $|\downarrow\rangle$ to shift upwards (from the gray, dashed level). When $|\downarrow\rangle$ and $|1\rangle$ are nearly degenerate, the two states hybridize, as shown in the middle of the panel, producing a minimum splitting of $2\hbar g_1$. (c) Structure of the Fe_8 SMM studied. (d) Photograph of an Fe_8 single crystal mounted in a cylindrical resonant cavity of radius 1.28 mm and depth 3.96 mm. Lines have been added to guide the eye. (e) Magnetic field lines for the TE_{011} resonant mode in the cavity.

$$H = DS_z^2 + E(S_x^2 - S_y^2) + C(S_+^4 + S_-^4) - g\mu_B \vec{B}_{\rm ext} \cdot \vec{S}, \tag{1}$$

where $\vec{B}_{\rm ext}$ is the externally applied magnetic field, $g \approx 2$, $D = -25.2$ eV, $E = -4.02$ eV, and $C = 7.4 \times 10^{-4}$ eV [38]. The first term in Eq. (1) makes the z axis the easy axis and defines the double-well potential. The spin has $2s + 1 = 21$ possible orientation states, $m = -10, -9, \ldots 10$ [levels in Fig. 1(a)]. The easy-axis field component B_z tilts the potential, as shown, and increases the energy differences between the lowest states.

Because of its anisotropy, an SMM's energy levels are typically anharmonically dispersed, as shown in Fig. 1(a), and so only one pair of spin levels will effectively couple to the cavity at a time. This pair then behaves as an effective spin-1/2 system. We relabel the lower (upper) of the relevant states as $|\uparrow\rangle$ ($|\downarrow\rangle$) and define $\hbar\omega_S$ as the energy difference between these two states. For example, when we truncate the states in Fig. 1(a) to the two lowest levels, we set $|\uparrow\rangle = |m = 10\rangle$ and $|\downarrow\rangle = |m = 9\rangle$.

The interaction of a two-level system with a cavity can be modeled by the Jaynes-Cummings Hamiltonian [39]:

$$H = H_{\rm spin} + H_{\rm rad} + H_{\rm int}, \tag{2}$$

where $H_{\rm spin} = (\hbar\omega_S/2)(1 - \sigma_z)$ is the spin Hamiltonian [i.e., Eq. (1) truncated to the two relevant levels], $H_{\rm rad} = \hbar\omega_C a^\dagger a$ is the Hamiltonian for the cavity mode, and $H_{\rm int} = (\hbar g_1/2)(a\sigma_- + a^\dagger\sigma_+)$ is the spin-photon interaction Hamiltonian. The σ's are standard Pauli spin matrices in the $\{|\uparrow\rangle, |\downarrow\rangle\}$ basis and $a^\dagger(a)$ is the photon creation (annihilation) operator for the cavity mode, acting on photon-number basis states $|n\rangle$. Offsets have been chosen to make the energy of the $|\uparrow\rangle|0\rangle$ ground state zero. The spin-radiation interaction strength g_1 is given by

$$g_1 = |\langle\uparrow|S_T|\downarrow\rangle| g\mu_B B_{\rm rf}/\hbar, \tag{3}$$

where $B_{\rm rf}$ is the radiative magnetic field of a single photon and S_T is the projection of the spin operator in the direction of $B_{\rm rf}$. The subscript 1 in g_1 indicates that a single spin is coupled to the cavity. With $n \leq 1$, the excited eigenstates of Eq. (2) are

$$\begin{aligned} |+\rangle &= \sin(\varphi/2)|\downarrow\rangle|0\rangle + \cos(\varphi/2)|\uparrow\rangle|1\rangle, \\ |-\rangle &= \cos(\varphi/2)|\downarrow\rangle|0\rangle - \sin(\varphi/2)|\uparrow\rangle|1\rangle, \end{aligned} \tag{4}$$

with energies

$$E_\pm = \frac{\hbar}{2}((\omega_C + \omega_S) \pm \sqrt{\Delta^2 + 4g_1^2}), \tag{5}$$

where $\Delta = \omega_C - \omega_S$ is the cavity-spin detuning and $\tan\varphi = 2g_1/\Delta$. Equation (5) describes two branches of a hyperbola with asymptotes $E = \hbar\omega_C$ and $E = \hbar\omega_S$. For large Δ, the excited eigenstates approach the independent excitation of the cavity or the spin [dashed gray level $|\downarrow\rangle$ in Fig. 1(b)], respectively, and the excited states of the total system are well described by $|\uparrow\rangle|1\rangle$ and $|\downarrow\rangle|0\rangle$. Applying an external magnetic field increases ω_S, raising the energy of the $|\downarrow\rangle$ state [from dashed to solid level in Fig. 1(b)]. When ω_S becomes close to ω_C [vertical dashed black line in Figs. 2(b),(c)], the spin will interact with the cavity mode and the system's excited states hybridize. At $\Delta = 0$ and with one excitation in the system, the splitting between the two branches, $E_+ - E_-$ is $2\hbar g_1$, the vacuum-Rabi splitting, and the excited states of the system become simply $|\pm\rangle = (1/\sqrt{2})(|\downarrow\rangle|0\rangle \pm |\uparrow\rangle|1\rangle)$, the two split states in Fig. 1(b).

Using the structure of our cavity mode, it is straightforward to calculate the single-photon field at the position of the sample to be $B_{\rm rf} = 3.7(6) \times 10^{-7}$ G. Equation (3) then yields $g_1/2\pi = 2.4$ Hz, much too small to be detected in a realistic experiment. As first shown by Tavis and Cummings [41], when N identical spins couple to the cavity, the interaction strength becomes

$$g_N = \sqrt{N} g_1. \tag{6}$$

The system's energies are still described by Eq. (5) with g_1 replaced by g_N and the eigenstates by Eq. (4) with $|\uparrow\rangle$ and $|\downarrow\rangle$ replaced, respectively, by $|\Uparrow\rangle = |\uparrow\uparrow\uparrow\ldots\uparrow\rangle$ and $|\Downarrow\rangle = (1/\sqrt{N})(|\downarrow\uparrow\uparrow\ldots\uparrow\rangle + |\uparrow\downarrow\uparrow\ldots\uparrow\rangle, + \ldots + |\uparrow\uparrow\uparrow\ldots\downarrow\rangle)$, where the latter describes an equal superposition of each spin being flipped into the excited state (while the remainder stay in the ground state). For the case relevant to our experiments, where

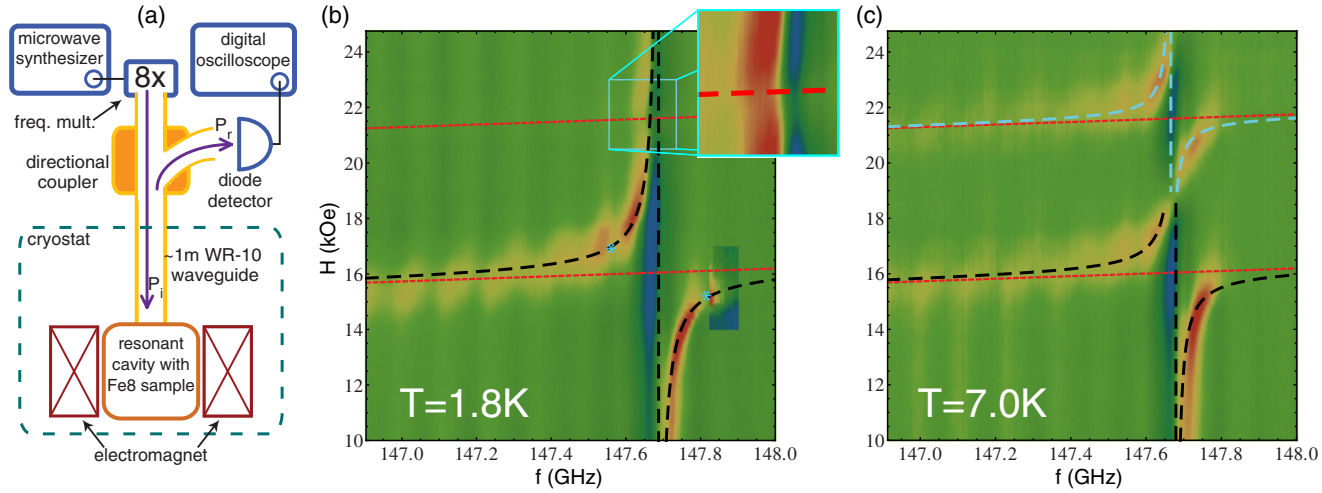

FIG. 2 (color online). Spectroscopic technique and results. (a) Schematic diagram of experimental apparatus. (b) and (c) Absorbed power as a function of magnetic field and radiation frequency at 1.8 and 7.0 K, respectively. Yellow and red indicate regions of significant power absorption. The dark blue regions are largely artificial, produced by our background-subtraction procedure [40]. The lower (upper) red dashed line is the Zeeman energy separation for the $m = 10$-to-9 (9-to-8) transition. The dashed black (cyan) curve is a fit of the data for the lower- (upper-)field data to Eq. (5). The outset of (b) shows a zoomed-in view of the boxed region with a slightly different coloring scheme. Similarly, the data within the lower boxed region in (b) are rendered with a different coloring scheme to emphasize the weaker features. In both (b) and (c), an essentially field-independent background was subtracted to enhance visual presentation [40].

$N \sim 10^{16}$ spins couple to a cavity mode, $g_N/2\pi$ is ~200 MHz, an easily detectable frequency splitting.

In coupling to the cavity, the collection of N spins behaves as one "superspin" with $s = N/2$ [42]. The spin state $|\Downarrow\rangle$ corresponds to a rotation of the superspin vector from the z axis (such that the z component of the spin is reduced by 1). In our experiment, the number of photons in the cavity n is on the order of 10^{10}. Nevertheless, Eq. (6) remains valid when the assumption $n \leq 1$ is replaced by the less stringent condition $n \ll N$. The latter corresponds to the limit in which the superspin's angle relative to the z axis remains small. The anharmonic limit, in which this angle is large, gives rise to superradiant states [42]. In practice, N depends on temperature and thereby permits *in situ* control of the coupling strength g_N.

Crystals of Fe_8 were synthesized using standard techniques. The crystal used for measurements was photographed under a microscope to determine its dimensions. Using those and the known unit cell for Fe_8 [43], we determined that the sample consists of $N_0 = 2.3(4) \times 10^{16}$ SMMs. Figure 1(d) shows a photograph of a single crystal of the Fe_8 SMM mounted in our cylindrical copper cavity. The TE_{011} mode of our cavity has a resonant frequency of 147.677(2) GHz and $Q \sim 4000$. For this mode, the oscillating magnetic field, shown in Fig. 1(e), is nearly perpendicular to the easy axis. The sample is mounted with its easy axis $\theta \sim 35°$ from the external dc magnetic field, which is parallel to the cavity's symmetry axis. Our experimental setup is shown schematically in Fig. 2(a). We performed measurements of the radiation power reflected from the cavity-sample system as a function of frequency and dc magnetic field at several temperatures between ~1.8 and 20 K.

Figures 2(b) and 2(c) show absorbed power at 1.8 and 7.0 K, respectively, for a range of frequencies and magnetic fields. Resonances of the system appear as yellow or red regions. The data exhibit two distinct resonant branches, each of which corresponds to one of the coupled spin-photon states in Eq. (4). At low magnetic fields, the resonances appear near the bare cavity resonance frequency (vertical dashed line) and the excitation frequency for the dipole-allowed $m = 10$-to-9 spin transition (lower red dashed line). When the field approaches the value at which these resonances would cross in the absence of interaction, a clear avoided crossing opens up with the upper-left branch curving and eventually approaching the cavity resonance frequency. The lower right branch tends towards the spin transition frequency but signal strength is lost as the frequency increases. Irrespective of this loss of signal, the upper left branch clearly transits smoothly between cavitylike and Zeeman-like behavior, indicating that the system has entered the so-called strong-coupling regime with states like those described by Eq. (4). Moreover, we find that there is a range of fields at which two resonance frequencies are observed [40], a telltale sign of strong coupling. Both branches can be fit very well by Eq. (5) (with g_1 replaced by g_N) as shown by the black dashed curves in Fig. 2(b) [40]. Only two parameters in the fit are unconstrained by the spin Hamiltonian or the cavity's resonant frequency: θ, the angle between the easy axis and the magnetic field, a parameter that was restricted to be the same at all temperatures, and g_N, which was allowed to vary with temperature. The former determines the slope of the spin transition frequency's field dependence (lower red dashed line) while the latter determines the gap between the

two branches of the hyperbola. Our fits provide a best value of $\theta = 37.7°$, close to the expected value of 35° based on the sample's orientation. For the data shown in Fig. 2(b), we obtain $g_N/2\pi = 0.519(4)$ GHz.

Figure 2(b) shows another, much smaller feature where the upper red dashed line, corresponding to the $m = 9$-to-8 transition, intersects the cavity frequency; the feature is highlighted in the outset. Since at 1.8 K there are far fewer molecules in the excited $m = 9$ state than in the $m = 10$ ground state, the value of N for the 9-to-8 transition is very small, resulting in a smaller coupling to the cavity mode. The splitting g_N for this transition can be increased by raising the temperature T and, thereby, N for the $m = 9$ state. Indeed, as shown in Fig. 2(c), increasing T to 7.0 K decreases the magnitude of the splitting associated with the (lower field) 10-to-9 transition and dramatically increases the coupling associated with the (higher field) 9-to-8 transition. This observation reflects the fact that raising the temperature monotonically reduces the population in the ground ($m = 10$) state while initially increasing the population of the excited ($m = 9$) state.

We fit the data in Fig. 2 (and similar data at other temperatures) to obtain values of g_N for each spin-cavity resonance at all temperatures for which a good fit to Eq. (5) could be obtained. g_N^2 should be proportional to the relative population $p = N/N_0$ for the relevant transition. In Fig. 3, we plot $(\hbar g_N/|\langle\uparrow|\vec{S}_T|\downarrow\rangle|\mu_B g)^2 = pN_0B_{rf}^2$ as a function of temperature for the two transitions measured. It is straightforward to calculate the populations p of the $m = 10$ and 9 states as a function of temperature with no adjustable parameters [40]. The solid curves in Fig. 3 show this temperature dependence for the relevant levels, $m = 10$ and $m = 9$. The agreement between the data and the corresponding populations is evident. The only adjustable parameter for these curves is the product of N_0 and B_{rf}^2, which determines the vertical scale of the curves. Taking $N_0 = 2.3 \times 10^{16}$, we determine $B_{\mathrm{rf}} = 5.30(1) \times 10^{-7}$ G for the 10-to-9 transition [Fig. 3(a)] and $4.98(3) \times 10^{-7}$ G for the 9-to-8 transition [Fig. 3(b)]. These values agree well with each other and are on the same order as our calculated value of $3.7(6) \times 10^{-7}$ G. The discrepancy may arise from modal mixing with the nearly degenerate TM_{111} mode.

Inhomogeneous broadening in Fe_8, as in many SMMs, arises from variations within a sample of the anisotropy parameter D, as well as other Hamiltonian parameters [37]. The broadening can be seen in the rather wide spin resonances in the data in Fig. 2, which have a Gaussian width of ~760 Oe [40], corresponding to a frequency width of $\sigma_\omega/2\pi \sim$ 1.7 GHz. A Gaussian distribution of N spin resonant frequencies ω_S is expected to still couple collectively if $\sigma_\omega \lesssim g_N$ [44–46]. Remarkably, our results do not quite meet this condition with $\sigma_\omega \gtrsim 3g_N$. In this regime, theory predicts a single S-shaped curve centered on the intersection of the Zeeman line with the cavity frequency (see [40]) instead of the two distinct branches that we observe in Figs. 2(b),(c). The light blue asterisks in Fig. 2(b) indicate the turning points of the predicted resonance curve, calculated following [45] and using the measured value of σ_ω and the value of g_N determined for that data set. The fact that the actual data do not show such turning points (most obvious in the left branch) indicates an unexpected collective coupling despite significant inhomogeneous broadening. This may be due to the existence of a small nonlinearity in the spin-cavity or spin-spin interactions that induces the spins to synchronize [47] as Δ becomes small, or the presence of some weak additional coupling mechanism, perhaps mediated by the crystal lattice [48]. These and other possible mechanisms are the subject of ongoing experimental and theoretical investigations. Regardless of the specific mechanism, our findings indicate that the spins need not have nearly identical resonant frequencies in order to couple collectively to a cavity mode but can do so even with substantial inhomogeneous broadening.

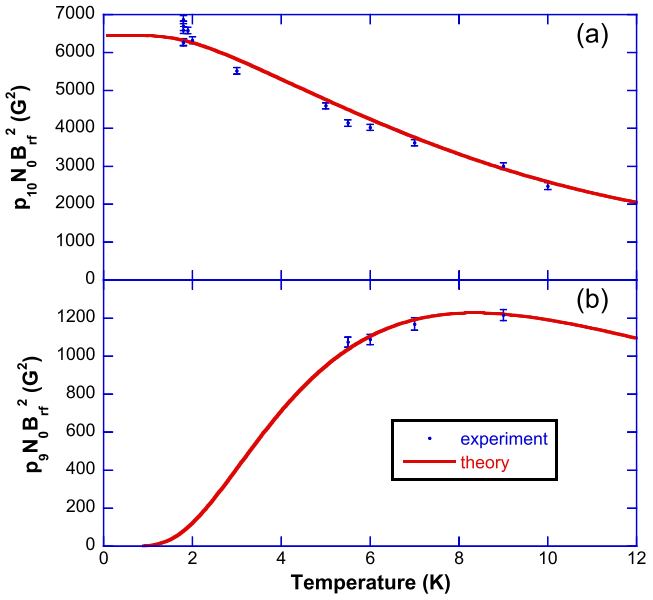

FIG. 3 (color online). Measured frequency splitting as a function of temperature for the (a) $m = 10$-to-9 transition and (b) $m = 9$-to-8 transition. The splitting has been recast in terms of the relative level population p of the lower level (see text) and compared with populations calculated using the known energy levels for the Fe_8 single-molecule magnet (solid curves).

We thank M. Bal for much useful advice and for his work on an earlier version of this experiment. We also thank E. M. Chudnovsky, J. A. Grover, D. S. Hall, D. B. Haviland, S. Hill, A. J. Millis, L. A. Orozco, M. P. Sarachik, D. I. Schuster, S. H. Strogatz, F. K. Wilhelm, and D. J. Wineland for useful discussions, and R. Cann for technical assistance and advice. Support for this work was provided by the National Science Foundation under Grants No. DMR-0449516, No. DMR-1006519, and No. DMR-1310135 and by the Amherst College Dean of Faculty.

*Present address: Department of Physics, 366 LeConte Hall #7300, Berkeley, CA 94720, USA.
†Present address: National High Magnetic Field Laboratory, 1800 E. Paul Dirac Drive, Tallahassee, FL 32310, USA.
‡Corresponding author. jrfriedman@amherst.edu

[1] R. Sessoli, D. Gatteschi, A. Caneschi, and M. A. Novak, Nature (London) **365**, 141 (1993).
[2] M. Mannini, F. Pineider, C. Danieli, F. Totti, L. Sorace, P. Sainctavit, M. A. Arrio, E. Otero, L. Joly, J. C. Cezar, A. Cornia, and R. Sessoli, Nature (London) **468**, 417 (2010).
[3] J. R. Friedman and M. P. Sarachik, Annu. Rev. Condens. Matter Phys. **1**, 109 (2010).
[4] M. N. Leuenberger and D. Loss, Nature (London) **410**, 789 (2001).
[5] A. Ardavan, O. Rival, J. J. L. Morton, S. J. Blundell, A. M. Tyryshkin, G. A. Timco, and R. E. P. Winpenny, Phys. Rev. Lett. **98**, 057201 (2007).
[6] S. Bertaina, S. Gambarelli, T. Mitra, B. Tsukerblat, A. Muller, and B. Barbara, Nature (London) **453**, 203 (2008).
[7] C. Schlegel, J. van Slageren, M. Manoli, E. K. Brechin, and M. Dressel, Phys. Rev. Lett. **101**, 147203 (2008).
[8] S. Takahashi, J. van Tol, C. C. Beedle, D. N. Hendrickson, L. C. Brunel, and M. S. Sherwin, Phys. Rev. Lett. **102**, 087603 (2009).
[9] H. B. Heersche, Z. de Groot, J. A. Folk, H. S. J. van der Zant, C. Romeike, M. R. Wegewijs, L. Zobbi, D. Barreca, E. Tondello, and A. Cornia, Phys. Rev. Lett. **96**, 206801 (2006).
[10] M.-H. Jo, J. E. Grose, K. Baheti, M. M. Deshmukh, J. J. Sokol, E. M. Rumberger, D. N. Hendrickson, J. R. Long, H. Park, and D. C. Ralph, Nano Lett. **6**, 2014 (2006).
[11] J. J. Henderson, C. M. Ramsey, E. del Barco, A. Mishra, and G. Christou, J. Appl. Phys. **101**, 09E102 (2007).
[12] S. Voss, M. Fonin, U. Rudiger, M. Burgert, and U. Groth, Appl. Phys. Lett. **90**, 133104 (2007).
[13] A. S. Zyazin, H. S. J. van der Zant, M. R. Wegewijs, and A. Cornia, Synth. Met. **161**, 591 (2011).
[14] S. Kahle, Z. Deng, N. Malinowski, C. Tonnoir, A. Forment-Aliaga, N. Thontasen, G. Rinke, D. Le, V. Turkowski, T. S. Rahman, S. Rauschenbach, M. Ternes, and K. Kern, Nano Lett. **12**, 518 (2012).
[15] M. Urdampilleta, S. Klyatskaya, J. P. Cleuziou, M. Ruben, and W. Wernsdorfer, Nat. Mater. **10**, 502 (2011).
[16] R. Vincent, S. Klyatskaya, M. Ruben, W. Wernsdorfer, and F. Balestro, Nature (London) **488**, 357 (2012).
[17] P. Rabl, D. DeMille, J. M. Doyle, M. D. Lukin, R. J. Schoelkopf, and P. Zoller, Phys. Rev. Lett. **97**, 033003 (2006).
[18] H. de Riedmatten, M. Afzelius, M. U. Staudt, C. Simon, and N. Gisin, Nature (London) **456**, 773 (2008).
[19] J. J. L. Morton, A. M. Tyryshkin, R. M. Brown, S. Shankar, B. W. Lovett, A. Ardavan, T. Schenkel, E. E. Haller, J. W. Ager, and S. A. Lyon, Nature (London) **455**, 1085 (2008).
[20] M. Blencowe, Nature (London) **468**, 44 (2010).
[21] X. Zhu, S. Saito, A. Kemp, K. Kakuyanagi, S.-i. Karimoto, H. Nakano, W. J. Munro, Y. Tokura, M. S. Everitt, K. Nemoto, M. Kasu, N. Mizuochi, and K. Semba, Nature (London) **478**, 221 (2011).
[22] M. Brune, F. Schmidt-Kaler, A. Maali, J. Dreyer, E. Hagley, J. M. Raimond, and S. Haroche, Phys. Rev. Lett. **76**, 1800 (1996).
[23] Y. Colombe, T. Steinmetz, G. Dubois, F. Linke, D. Hunger, and J. Reichel, Nature (London) **450**, 272 (2007).
[24] J. P. Reithmaier, G. Sek, A. Loffler, C. Hofmann, S. Kuhn, S. Reitzenstein, L. V. Keldysh, V. D. Kulakovskii, T. L. Reinecke, and A. Forchel, Nature (London) **432**, 197 (2004).
[25] T. Yoshie, A. Scherer, J. Hendrickson, G. Khitrova, H. M. Gibbs, G. Rupper, C. Ell, O. B. Shchekin, and D. G. Deppe, Nature (London) **432**, 200 (2004).
[26] A. Wallraff, D. I. Schuster, A. Blais, L. Frunzio, R. S. Huang, J. Majer, S. Kumar, S. M. Girvin, and R. J. Schoelkopf, Nature (London) **431**, 162 (2004).
[27] A. Imamoğlu, Phys. Rev. Lett. **102**, 083602 (2009).
[28] E. Abe, H. Wu, A. Ardavan, and J. J. L. Morton, Appl. Phys. Lett. **98**, 251108 (2011).
[29] I. Chiorescu, N. Groll, S. Bertaina, T. Mori, and S. Miyashita, Phys. Rev. B **82**, 024413 (2010).
[30] Y. Kubo, F. R. Ong, P. Bertet, D. Vion, V. Jacques, D. Zheng, A. Dréau, J. F. Roch, A. Auffeves, F. Jelezko, J. Wrachtrup, M. F. Barthe, P. Bergonzo, and D. Esteve, Phys. Rev. Lett. **105**, 140502 (2010).
[31] R. Amsüss, C. Koller, T. Nöbauer, S. Putz, S. Rotter, K. Sandner, S. Schneider, M. Schramböck, G. Steinhauser, H. Ritsch, J. Schmiedmayer, and J. Majer, Phys. Rev. Lett. **107**, 060502 (2011).
[32] H. Wu, R. E. George, J. H. Wesenberg, K. Mølmer, D. I. Schuster, R. J. Schoelkopf, K. M. Itoh, A. Ardavan, J. J. L. Morton, and G. A. D. Briggs, Phys. Rev. Lett. **105**, 140503 (2010).
[33] D. I. Schuster, A. P. Sears, E. Ginossar, L. DiCarlo, L. Frunzio, J. J. L. Morton, H. Wu, G. A. D. Briggs, B. B. Buckley, D. D. Awschalom, and R. J. Schoelkopf, Phys. Rev. Lett. **105**, 140501 (2010).
[34] S. Probst, H. Rotzinger, S. Wünsch, P. Jung, M. Jerger, M. Siegel, A. V. Ustinov, and P. A. Bushev, Phys. Rev. Lett. **110**, 157001 (2013).
[35] V. Ranjan, G. de Lange, R. Schutjens, T. Debelhoir, J. P. Groen, D. Szombati, D. J. Thoen, T. M. Klapwijk, R. Hanson, and L. DiCarlo, Phys. Rev. Lett. **110**, 067004 (2013).
[36] K. M. Mertes, Y. Suzuki, M. P. Sarachik, Y. Paltiel, H. Shtrikman, E. Zeldov, E. Rumberger, D. N. Hendrickson, and G. Christou, Phys. Rev. Lett. **87**, 227205 (2001).
[37] S. Hill, S. Maccagnano, K. Park, R. M. Achey, J. M. North, and N. S. Dalal, Phys. Rev. B **65**, 224410 (2002).
[38] R. Caciuffo, G. Amoretti, A. Murani, R. Sessoli, A. Caneschi, and D. Gatteschi, Phys. Rev. Lett. **81**, 4744 (1998).
[39] E. T. Jaynes and F. W. Cummings, Proc. IEEE **51**, 89 (1963).
[40] See Supplemental Material at http://link.aps.org/supplemental/10.1103/PhysRevLett.112.120501 for details of data acquisition and analysis.
[41] M. Tavis and F. W. Cummings, Phys. Rev. **170**, 379 (1968).
[42] R. H. Dicke, Phys. Rev. **93**, 99 (1954).
[43] K. Weighardt, K. Pohl, I. Jibril, and G. Huttner, Angew. Chem., Int. Ed. Engl. **23**, 77 (1984).
[44] R. Houdré, R. P. Stanley, and M. Ilegems, Phys. Rev. A **53**, 2711 (1996).
[45] I. Diniz, S. Portolan, R. Ferreira, J. M. Gérard, P. Bertet, and A. Auffèves, Phys. Rev. A **84**, 063810 (2011).
[46] Z. Kurucz, J. H. Wesenberg, and K. Mølmer, Phys. Rev. A **83**, 053852 (2011).
[47] R. Mirollo and S. Strogatz, SIAM J. Appl. Math. **50**, 1645 (1990).
[48] E. M. Chudnovsky and D. A. Garanin, Phys. Rev. Lett. **93**, 257205 (2004).

Supplemental Material for "Collective coupling of a macroscopic number of single-molecule magnets with a microwave cavity mode"

A. W. Eddins,[1] C. C. Beedle,[2] D. N. Hendrickson,[2] and Jonathan R. Friedman[1]

[1]*Department of Physics, Amherst College, Amherst, MA 01002-5000*

[2]*Department of Chemistry & Biochemistry, University of California at San Diego, La Jolla, CA 92093*

The broadband detector employed in our apparatus contains an inverting diode so that higher levels of power absorption (indicative of resonances of the system) appear as peaks in the data rather than as troughs. Thus, the data can be simply interpreted as representing absorbed power relative to an unimportant offset.

The upper panel in Fig. 1 shows raw data for absorbed power as a function of frequency and magnetic field at 7.0 K. The vertical bands in the figure are due to low-finesse resonances of our probe's waveguide, resulting in a roughly sinusoidal variation of power with frequency. While the signal from these background resonances varies significantly with frequency, it depends weakly on the applied magnetic field. It is straightforward to largely remove the background signal by taking the frequency dependence at low or high magnetic fields, i.e. far from where the sample interacts with the cavity, as reference data and subtracting it off from the data at all fields. Such an operation (followed by adjustments to color scale for visual clarity) performed on the 1.8 and 7.0 K data yields Figs. 2b and 2c (in the main text), respectively. The subtraction procedure results in the artificial dark blue regions in those figures because the procedure subtracts the bare cavity resonance from the data. We emphasize that these figures are produced for purposes of visually displaying the data. Actual data analysis was done on the raw data, as we explain presently.

Since the background is largely independent of magnetic field, we can isolate the spin resonance peaks from the background by analyzing constant-frequency subsets of the data. The lower panels of Fig. 1 show constant-frequency slices (along the thin vertical dashed lines in the upper panel) of absorbed power as a function of field. Two peaks are clearly visible, the lower-field one corresponding to the 10-to-9 transition and the higher-field one corresponding to the 9-to-8 transition. Some field dependence in the background is also observed. To find the position of each peak (magnetic field value for the resonance), we separately fit the data in the vicinity of each peak to a Gaussian plus a line, the latter to account for the variation of the background. Such a fit provides resonant-field values and uncertainties at each value of frequency. The peak positions obtained in this way for one data set are shown by the orange and green points in the upper panel of Fig. 2. The fitting procedure returned a small number of clearly spurious data points, which were omitted from subsequent analysis. The oscillations in the peak positions as a function of frequency are remnants of background effects that were not fully accounted for by our fitting procedure. Because the magnitude of these background fluctuations is generally much larger than the uncertainties in the measured peak positions, we neglected these uncertainties in subsequent fitting.

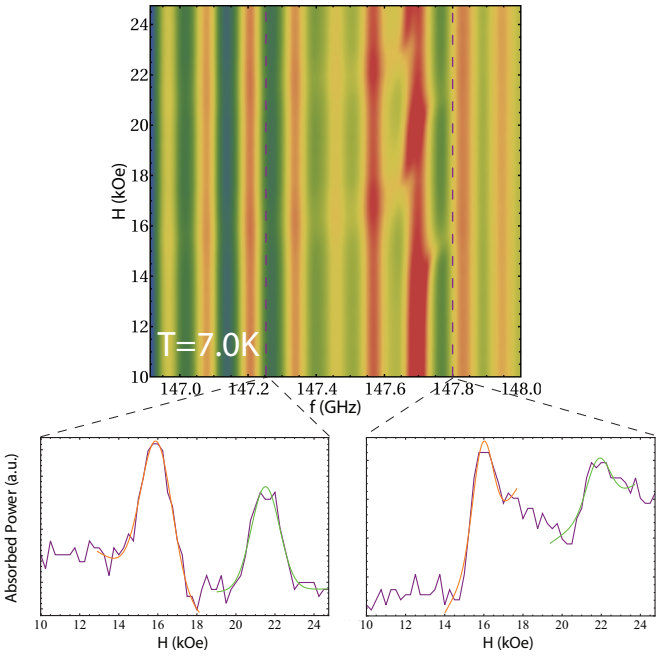

FIG. 1. Absorbed power as a function of frequency and magnetic field at T = 7.0 K. The lower panels show absorbed power as a function of magnetic field for a fixed frequency, i.e. data along the indicated vertical dashed line in the top panel. The orange and green curves are fits to a Gaussian plus a line, the latter to account for the behavior of the background. The vertical scales for the two lower panels are somewhat different.

We next fit the frequency dependence of the peak field positions. The expected dependence can be obtained from Eq. 4 (main text) and the very good approximation that the spin resonance frequency, $f_S = \omega_S/2\pi$ depends linearly on field: $f_S = f_0 + \beta H$. Making this substitution in Eq. 4 and solving for H yields

$$H = \frac{1}{\beta}\left(\frac{(g_N/2\pi)^2}{f_C - f} + f - f_0\right), \tag{1}$$

where $f = \omega/2\pi$ is the resonance frequency of the coupled system and $f_C = \omega_C/2\pi$ is the bare-cavity resonance frequency. The constants f_0 and β depend on the anisotropy parameters of the Hamiltonian and the angle θ between the easy axis and the magnetic field. f_0 and β depend weakly

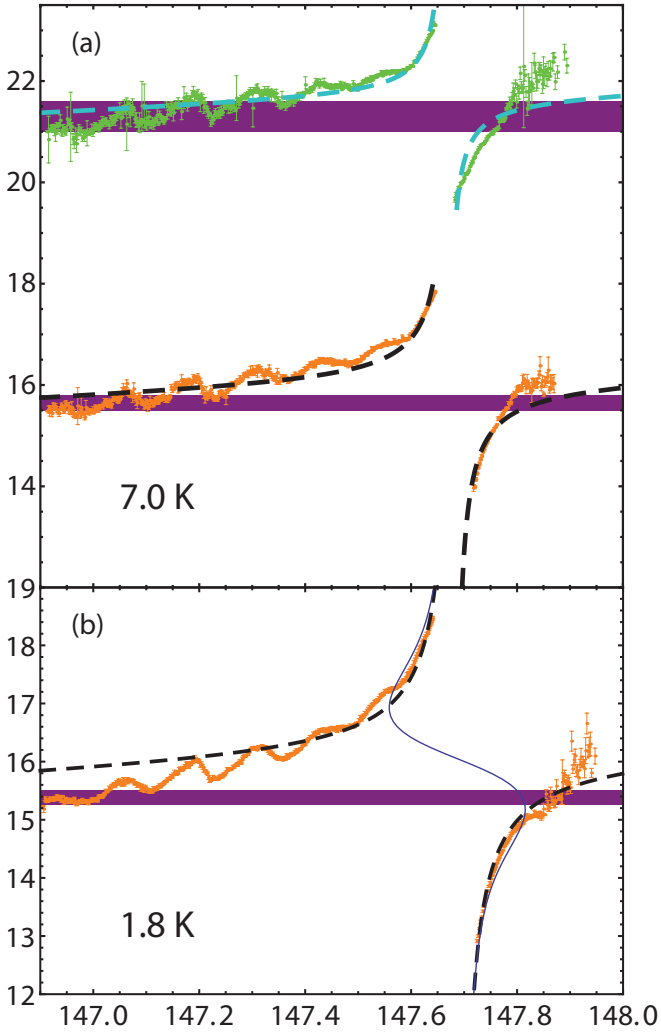

FIG. 2. Resonance peak positions as a function of frequency (orange and green points) determined from fitting the data, as described in the text. Data for (a) 7.0 K (obtained from an analysis of Fig. 1) and (b) 1.8 K are shown. The oscillations of the peak positions are due to remnant effects of the frequency-dependent background. The data are fit (dashed lines) to Eq. 1. The shaded regions indicate the ranges of magnetic fields over which the system unambiguously exhibits two resonant frequencies. The blue curve in (b) shows the expected field dependence of the resonance given the measured inhomogeneous broadening of the spin resonance.

on the azimuthal angle ϕ, which determines the orientation of the field in relation to the intermediate (x) axis of the Fe_8 molecule. The dependence on ϕ is sufficiently weak that it is not a reliable fitting parameter and we simply fixed ϕ at the expected value of 108.7°, based on the crystal's orientation. We set the Hamiltonian parameters at the values given in the main text and let θ be a free parameter. $f_0(\theta)$ and $\beta(\theta)$ were then calculated by diagonalizing the Hamiltonian to obtain its eigenenergies, then determining the frequency f_S for the relevant (e.g. 10-to-9) resonance as a function of H and θ, and fitting the H dependence to a line in the experimentally relevant range of field values. Eq. 1 was simultaneously fit to the resonance peak positions corresponding to the relevant spin resonance with θ, f_C and g_N as fitting parameters. θ was forced to be the same for each data set while f_C and g_N were allowed to vary from one data set to the next. Our fits yielded $\theta = 37.7°$ and a separate best-fit value of g_N for each data set. The upper panel of Fig. 2 shows the peak-position data obtained from the data shown in Fig. 1 and the resulting fit to Eq. 1, following the procedures described above. The lower panel in Fig. 2 results from applying a similar procedure to data at 1.8 K. At that low temperature, the higher-field (9-to-8) resonance does not display an unambiguous splitting and only the signal from the lower-field (10-to-9) resonance was analyzed.

The values of f_C obtained from our fits show a variation with temperature on the order of 10 MHz. f_C values for the 9-to-8 resonance were generally somewhat smaller than those for the 10-to-9 resonance. This weak behavior is likely due to a combination of changes in mean dipolar fields with temperature and the remnant effect of one spin-cavity interaction on the other one. Neither of these effects is significant enough to substantially impact our main conclusions.

One important feature of the data is the fact that for some regions of field, the system has two distinct resonant frequencies, as illustrated in Fig. 2 by the shaded regions. This observation indicates that the spin-cavity system is in the so-called strong-coupling regime.

The blue curve in Fig. 2(b) shows the predicted behavior of the resonance peak, given the measured amount of inhomogeneous broadening (σ_ω) and assuming a Gaussian inhomogeneous lineshape, as discussed in the main text. The actual data clearly does not follow this predicted behavior. The turning points of this curve are marked by the light blue asterisks in Fig. 2(b) of the main text.

The values of g_N obtained from our fitting procedure are plotted in Fig. 3 (main text) and fit to the energy-level populations with one adjustable parameter, as described in the main text. In our population calculations, we also included levels in the known s = 9 spin manifold for Fe_8 [1].

[1] D. Zipse, J. M. North, N. S. Dalal, S. Hill, and R. S. Edwards, Phys. Rev. B **68**, 184408 (2003).